CHEMISTRY
A European Journal

A Journal of
ChemPubSoc Europe

Accepted Article

Title: Vibrational Quenching in Near-Infrared Emitting Lanthanide Complexes: A Quantitative Experimental Study and Novel Insights

Authors: Flavia Artizzu, Dimitrije Mara, Philippe F. Smet, Anna M. Kaczmarek, Kristof Van Hecke, and Rik Van Deun

To be cited as: *Chem. Eur. J.* 10.1002/chem.201904320

Link to VoR: http://dx.doi.org/10.1002/chem.201904320

Supported by
ACES

WILEY-VCH

10.1002/chem.201904320

WILEY-VCH

FULL PAPER

Vibrational Quenching in Near-Infrared Emitting Lanthanide Complexes: A Quantitative Experimental Study and Novel Insights

Dimitrije Mara,[a,b] Flavia Artizzu, *[a] Philippe F. Smet,[c] Anna M. Kaczmarek,[d] Kristof Van Hecke,[b] and Rik Van Deun[a]

Abstract: Two series of novel NIR-emissive complexes of Nd^{3+}, Sm^{3+}, Er^{3+} and Yb^{3+} with two different b-diketonate ligands (L_1 = 4,4,4-trifluoro-1-phenyl-1,3-butadione and L_2 = 4,4,4-trifluoro-1-(4-chlorophenyl)-1,3-butadione) are reported. The neutral triphenylphosphine oxide (tppo) ligand was used to replace coordinated water molecules in the first coordination sphere of the as-obtained $[Ln(L_{1(2)})_3(H_2O)_2]$ complexes to afford water-free $[Ln(L_{1(2)})_3(tppo)_2]$ molecular species. Upon replacement of water molecules by tppo units, the NIR emission lifetimes of the Nd^{3+}, $Er^{3+}$and Sm^{3+}complexes increase by about one order of magnitude up to values of ~9, 8 and 113 ms while Yb^{3+} complexes reach intrinsic quantum yields as high as to Φ_{Yb} = 6.5%., which are remarkably high for fully hydrogenated complexes. Vibrational quenching by CH and OH oscillators has been quantitatively assessed by implementing the Förster's model of resonance energy transfer on the basis of experimental data. This study demonstrates that highly efficient NIR-emitting lanthanide complexes can be obtained with facile, cheap and accessible syntheses through a rational design.

[a] Mr D. Mara, Prof. R. Van Deun and Dr F. Artizzu
L^3 – Luminescent Lanthanide Lab, Department of Chemistry
Ghent University
Krijgslaan 281 – S3, B-9000, Ghent, Belgium.
E-mail: flavia.artizzu@ugent.be
[b] Mr D. Mara, Prof. K. Van Hecke
XStruct, Department of Chemistry
Ghent University
Krijgslaan 281 – S3, B-9000, Ghent, Belgium.
[c] Prof. P. F. Smet
LumiLab, Department of Solid State Sciences
Ghent University
Krijgslaan 281 – S1, B-9000, Ghent, Belgium.
[d] Dr A. M. Kaczmarek
COMOC – Center for Ordered Materials Organometallics and Catalysis, Department of Chemistry
Ghent University
Krijgslaan 281 – S3, B-9000, Ghent, Belgium.

Supporting information for this article is given via a link at the end of the document. It contains crystal data and refinement details, FTIR and ESI-MS data, photoluminescence spectra, absorption cross-section and overlap integrals evaluation.

Introduction

Near-infrared (NIR) lanthanide(III) (Nd^{3+}, Sm^{3+}, Pr^{3+}, Er^{3+}, Yb^{3+}) complexes are extensively studied as they are of great interest in applications such as in lasers, optical telecommunication, bioimaging, and many others.[1-4] The lanthanide ions (Ln) emission stems from intra-shell f-f transitions which are forbidden by Laporte's rule and as a result luminescence is characterized by long lifetimes and narrow bands. In molecular complexes, the weak absorption and consequently weak emission intensity of Ln ions can be overcome by the use of a sensitizing ligand, able to harvest light with high efficiency and transfer it to the metal (antenna-effect). However, the luminescence lifetimes achievable in NIR-emitting Ln complexes are greatly shortened by vibrational quenching phenomena mainly as a result of Förster's resonance energy transfer (FRET) to resonantly oscillating C-H and O-H groups present in the coordination environment.[5] This non-radiative dipolar through-space mechanism is dependent on the spectral resonance and the distance between the donor and acceptor oscillators and is particularly effective in the case of NIR-emitting Ln complexes as the low quanta superior harmonics and combinations of the vibrational modes of C-H groups and/or water/solvent molecules in the first coordination sphere are strongly resonant with the emission. This drawback indeed represents a severe limitation to the application of such materials. The design of NIR lanthanide complexes with high emission performances still represents a difficult challenge as it requires embedding the Ln emitter in a low-phonon environment devoid of

C-H and O-H (and N-H) quenchers in close proximity. [6-8] Finding an efficient antenna ligand free of these groups is a tricky task and many researchers have resorted to often cumbersome and cost-ineffective syntheses of deuterated or fluorinated organic molecules to achieve a significant improvement of the emission lifetimes.[7,9] However, despite two decades of research in this field, only rare examples of NIR-emitting Ln (Er^{3+} and Yb^{3+}) complexes displaying lifetimes of one or two orders of magnitude longer than usual values (hundreds of μs vs. 1-10 μs) have been so far reported, and in most cases the observed values are still far below those expected from the 'natural' radiative lifetime of the Ln emitter (usually falling in the ms time scale) in the absence of any quenching process.[9] This claims for a deeper understanding of vibrational quenching in Ln complexes which so far still remains largely unclear. A number of studies have been reported on the quantification of this phenomenon in NIR-emitting materials based on predictive theoretical models[10,11] or indirect evidence[12,13,14a] through systematic time-resolved measurements but little work has been done on the direct implementation of the Förster's model on the basis of experimental data, especially in regard to the assessment of the resonance condition necessary to allow for energy transfer. Moreover, while considerable attention has been devoted to the vibrational quenching of Er^{3+} emission, little information is available on other relevant NIR-emitting ions, such as Nd^{3+} and Yb^{3+}, while Sm^{3+} has been so far neglected in these studies.

In this work, we report an extensive and systematic experimental investigation on the synthesis, structure and luminescence performances in the NIR of two series of new tris β-diketonate complexes with 4,4,4-trifluoro-1-phenyl-1,3-butadionate and 4,4,4-trifluoro-1-(4-chlorophenyl)-1,3-butadionate, with water molecules or triphenylphosphine (tppo) units completing the coordination sphere, and we examine in detail the factors governing the vibrational quenching by high-energy O-H and C-H oscillators in the framework of the Förster's model of resonance energy transfer. Beside the all known and most popular NIR triad (Nd^{3+}, Er^{3+} and Yb^{3+}) in our study we have also included Sm^{3+} which, despite its interesting emission features displaying intense bands in the telecommunication window, has not been so far much studied in the NIR region.[14]

Results and Discussion

Synthesis and molecular structures. β-diketones are very popular ligands for luminescent Ln complexes since they are cheap, easy to synthesize (or are commercially available), can act as efficient antennas for Ln emission in the visible and near-infrared (NIR) regions and form stable complexes typically with high color purity thanks to the wide spectral gap between the ligand and the Ln optical features. In addition, their simple molecular backbone allows for tailoring the substituents and lower the degrees of freedom of the nature of organic quenchers present, for example aromatic and aliphatic C-H groups, thus making this class of molecules particularly suitable for our study.[15-17] In particular we selected the 4,4,4-trifluoro-1-phenyl-1,3-butadionate (L_1) and the 4,4,4-trifluoro-1-(4-chlorophenyl)-1,3-butadionate (L_2) ligands, both bearing a trifluoromethane group, supposed not to have a relevant role in vibrational quenching together with a phenyl ring with no substituents (L_1) and a chlorine atom in the para-position (L_2) reducing the number of aromatic C-H quenchers present in the molecular structure.

The β-diketonate complexes were synthesized by directly reacting the ligand in the deprotonated form (by addition of sodium hydroxide) with the appropriate lanthanide ion (Ln^{3+}) in stoichiometric ratio in methanol solution. The high reactivity of the β-diketonate ligands toward coordination to Ln^{3+} prevents the formation of the insoluble lanthanide hydroxides even under basic conditions. Complexes of general formula **$[Ln(L_1)_3(H_2O)_2]$** and **$[Ln(L_2)_3(H_2O)_2]$** were isolated for Ln = Nd^{3+}, Sm^{3+}, Er^{3+} and Yb^{3+}. The successive reaction of these hydrated β-diketonate complexes with the triphenylphosphinoxide (tppo) under mild conditions in methanol solution afforded water-free complexes of general formula **$[Ln(L_1)_3(tppo)_2]$** and **$[Ln(L_2)_3(tppo)_2]$** (Ln = Nd^{3+}, Sm^{3+}, Er^{3+} and Yb^{3+}). Neutral tppo moieties easily replace directly coordinated water molecules likely due to extra-stabilization stemming from the introduction of additional phenyl rings establishing π-π interactions with the phenyl ring from the β-diketonate ligands. As a consequence, the formation of complexes with tppo units in the first coordination sphere is favored over the water-coordinated derivatives although the increased steric hindrance may cause a possible spatial rearrangement of the ligands in the first coordination sphere. All compounds were characterized with analytical (elemental analysis, mass spectrometry) and spectroscopic (vibrational, electronic) methods as described in the Experimental Section. Structural studies by X-ray diffraction were performed on selected samples where suitable single crystals were available. Single crystal X-ray analysis revealed that **$[Nd(L_1)_3(H_2O)_2]$** adopts the configuration of a mononuclear tris β-diketonate complex with two water molecules in the first coordination sphere and crystallizes in the orthorhombic non-centrosymmetric space group $P2_12_12_1$. The Nd^{3+} ion is octa-coordinated by six oxygen atoms from three L_1 ligands and two oxygen atoms from water molecules (Figure 1 (a)) and the coordination polyhedron can be described as distorted square antiprism. The Yb^{3+} derivative with ligand L_2 is the only example where the crystal structure reveals the presence of a coordinated methanol molecule, which we attribute to the slightly different recrystallization conditions from a mixture of methanol/acetonitrile instead of a methanolic solution, which only afforded small crystals unsuitable for X-Ray structural studies. It is however noted that analytical results (CHN and ESI-mass, see SI) for the product recrystallized from methanol are in agreement with the **$[Yb(L_2)_3(H_2O)_2]$** formula. The structurally-characterized product consists of a mononuclear tris β-diketonate complex bearing one molecule of water and one of methanol in the first coordination sphere. The compound crystallizes in the triclinic centrosymmetric space group $P\bar{1}$ and the coordination geometry of the Yb^{3+} ion can be described as a distorted square antiprism defined by six oxygen atoms from three L_2 ligands and two oxygen atoms from directly bonded water and methanol molecules, reaching the coordination number of eight (Figure 2). For the tppo-containing complexes, the crystal structures of the Nd^{3+} derivative with ligand L_1 and the Sm^{3+} analogs with ligands L_1 and L_2 were

10.1002/chem.201904320

solved. The structures of **[Nd(L$_1$)$_3$(tppo)$_2$]** (Figure 1 (b)) and **[Sm(L$_1$)$_3$(tppo)$_2$]** (Figure S2 in SI) were found to be isomorphous and the former is briefly described herein as representative. The compound is a mononuclear tris β-diketonate complex bearing two neutral tppo molecules which excluded water molecules from the first coordination sphere. The compound crystallizes in the triclinic centrosymmetric space group $P\bar{1}$ and the Ln ion reaches a coordination number of eight by adopting a square antiprism coordination geometry defined by six oxygen atoms from three L_1 ligands and two oxygen atoms from two tppo neutral units acting as monodentate donors. **[Sm(L$_2$)$_3$(tppo)$_2$]** adopts a very similar arrangement as the analog with ligand L_1, crystallizing in the triclinic centrosymmetric $P\bar{1}$ space group as a mononuclear tris β-diketonate complex with two neutral tppo molecules to reach a coordination number of eight. Also in this case, the coordination geometry around Sm^{3+} is a square antiprism as defined by six oxygen donors from three bidentate monoanionic L_2 ligands and two monodentate tppo neutral units (Figure S3 in SI). Crystal data and refinement details can be found in Table S1 in SI.

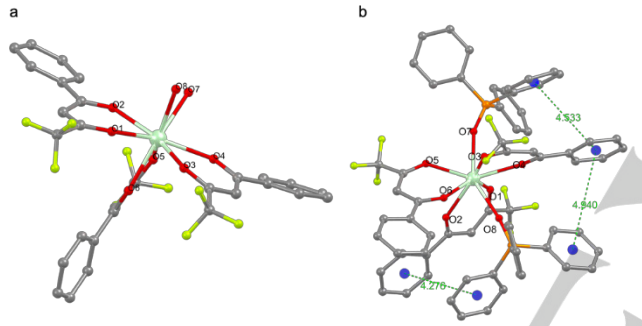

Figure 1. Molecular structures of **[Nd(L$_1$)$_3$(H$_2$O)$_2$]** (a) and **[Nd(L$_1$)$_3$(tppo)$_2$]** (b) in ball-stick representation, showing atom-labelling of the first coordination sphere around Nd^{3+}. Green dashed lines indicate π-π interactions between the phenyl rings of L_1 and tppo at distances in the range of 4.276(2)-4.940(2) Å.

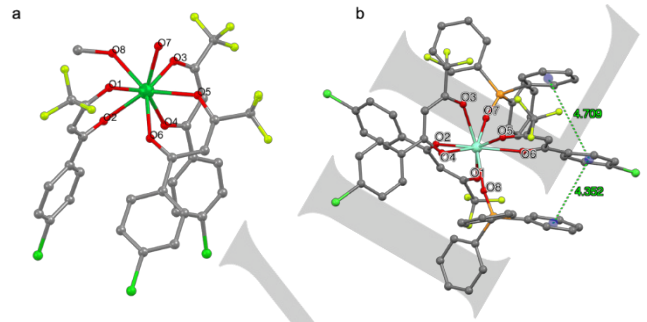

Figure 2. Molecular structure of **[Yb(L$_2$)$_3$(H$_2$O)(CH$_3$OH)]** (a) and **[Sm(L$_2$)$_3$(tppo)$_2$]** (b) in ball-stick representation, (a) showing atom-labeling of the first coordination sphere around the metal ion. Green dashed lines indicate π-π interactions between the phenyl rings of L_2 and tppo at distances in the range 4.352(5)-4.709(4) Å. Co-crystallized solvent molecules were removed for clarity.

The same stoichiometry and molecular arrangement was confirmed for all lanthanide analogs of the same class of complexes, as demonstrated by electro-spray ionization mass spectrometry (ESI-MS) and Fourier Transform infrared spectroscopy (FT-IR) investigation (see SI Figure S4-S24).

Steady-state and time-resolved photoluminescence (PL) studies. Upon excitation in the β-diketonate absorption band with UV light, all the studied complexes display NIR-emission with the characteristic emission peaks of the Er^{3+}, Nd^{3+}, Yb^{3+} and Sm^{3+} (Figure S28 in SI). In Figure 3a and 3b the photoluminescence (PL) spectra of **[Er(L$_1$)$_3$(H$_2$O)$_2$]** and **[Er(L$_1$)$_3$(tppo)$_2$]** complexes are presented. As it can be seen the intensity of the $^4I_{13/2} \rightarrow {}^4I_{15/2}$ emission peak at 1530 nm in **[Er(L$_1$)$_3$(H$_2$O)$_2$]** is hardly detected, as a consequence of the coordination environment around Er^{3+} in the complex, bearing two water molecules and accounting for the strong emission quenching. On replacement of the two water molecules by tppo ligands the emission intensity of the $^4I_{13/2} \rightarrow {}^4I_{15/2}$ transition band at 1530 nm increases significantly and the emission peak related to the $^4I_{11/2} \rightarrow {}^4I_{15/2}$ transition at 988 nm is detected. Similarly, the emission spectra of **[Er(L$_2$)$_3$(H$_2$O)$_2$]** and **[Er(L$_2$)$_3$(tppo)$_2$]**, depicted in Figure 3c and 3d, both display the characteristic peak of Er^{3+} $^4I_{13/2} \rightarrow {}^4I_{15/2}$ transition at 1530 nm while the $^4I_{11/2} \rightarrow {}^4I_{15/2}$ line at 989 nm only becomes visible for **[Er(L$_2$)$_3$(tppo)$_2$]**. The enhancement of the emission intensity of **[Er(L$_2$)$_3$(tppo)$_2$]** with respect to **[Er(L$_2$)$_3$(H$_2$O)$_2$]** is again remarkable as a consequence of the removal of H_2O molecules, but it is not as significant as it was in the case of **[Er(L$_1$)$_3$(H$_2$O)$_2$]** and **[Er(L$_1$)$_3$(tppo)$_2$]**. This finding can be explained by taking into consideration that the chlorine atom in the *para*- position of the phenyl ring has negative inductive effects and positive resonance effects on the π electrons of the ring.[18] These effects can induce a lowering of the excited energy levels of the ligand leading to a better energy match with the receiving upper levels of the Ln^{3+} ion and thus increasing the sensitization efficiency. Similar considerations can be made for the spectra of the Nd^{3+}, Sm^{3+} and Yb^{3+} derivatives. In the emission spectra of **[Nd(L$_1$)$_3$(H$_2$O)$_2$]**, **[Nd(L$_1$)$_3$(tppo)$_2$]**, **[Nd(L$_2$)$_3$(H$_2$O)$_2$]** and **[Nd(L$_2$)$_3$(tppo)$_2$]**, (Figure S25 in SI) the three characteristic emission peaks of Nd^{3+} appear at 885 nm ($^4F_{3/2} \rightarrow {}^4I_{9/2}$), 1060 nm ($^4F_{3/2} \rightarrow {}^4I_{11/2}$) and at 1300 nm ($^4F_{3/2} \rightarrow {}^4I_{13/2}$) upon ligand excitation. Samarium is a rare case of luminescent lanthanide ion emitting both in the visible and NIR region and the PL spectra of **[Sm(L$_1$)$_3$(H$_2$O)$_2$]**, **[Sm(L$_1$)$_3$(tppo)$_2$]**, **[Sm(L$_2$)$_3$(H$_2$O)$_2$]** and **[Sm(L$_2$)$_3$(tppo)$_2$]** (Figure S26 in SI) display all the characteristic emission peaks originating from the decay of the same $^4G_{5/2}$ excited level of Sm^{3+} at 883 nm ($^4G_{5/2} \rightarrow {}^6F_{1/2}$), 905 nm ($^4G_{5/2} \rightarrow {}^6F_{3/2}$), 920 nm ($^4G_{5/2} \rightarrow {}^6H_{15/2}$), 950 nm ($^4G_{5/2} \rightarrow {}^6F_{5/2}$), 1000 nm and 1031 nm (split peak for the $^4G_{5/2} \rightarrow {}^6F_{7/2}$ transition), 1178 nm ($^4G_{5/2} \rightarrow {}^6F_{9/2}$), 1298 nm and 1425 nm ($^4G_{5/2} \rightarrow {}^6F_{11/2}$). Also in this case, the **[Sm(L$_1$)$_3$(tppo)$_2$]** and **[Sm(L$_2$)$_3$(tppo)$_2$]** emission peaks are of higher intensity in comparison with the complexes with water molecules and there is evident resolution into a fine structure of the peaks at 883 nm ($^4G_{5/2} \rightarrow {}^6F_{1/2}$) and at 905 nm ($^4G_{5/2} \rightarrow {}^6F_{3/2}$) as a consequence of the change in the environment of Sm^{3+} on going from water to tppo coordination. An opposite trend is instead observed for Yb^{3+} emission at 977 nm ($^2F_{5/2} \rightarrow {}^2F_{7/2}$) in **[Yb(L$_1$)$_3$(tppo)$_2$]** and **[Yb(L$_2$)$_3$(tppo)$_2$]** with respect to **[Yb(L$_1$)$_3$(H$_2$O)$_2$]** and **[Yb(L$_2$)$_3$(H$_2$O)$_2$]** (Figure S27 in SI) as the Stark splitting is more evident and resolved for the water-

10.1002/chem.201904320

containing complexes whereas the change in intensity between the two series of compounds, while still significant, is much smaller than that observed for the Nd^{3+}, Er^{3+} and Sm^{3+} derivatives.

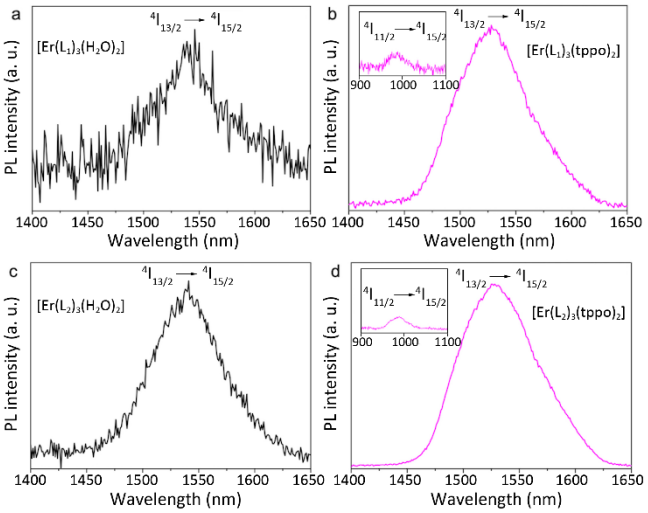

Figure 3. PL emission spectra of Er^{3+} in **[Er(L₁)₃(H₂O)₂]** (a), **[Er(L₁)₃(tppo)₂]** (b), **[Er(L₂)₃(H₂O)₂]** (c) and **[Er(L₂)₃(tppo)₂]** (d) upon excitation in the ligand absorption band.

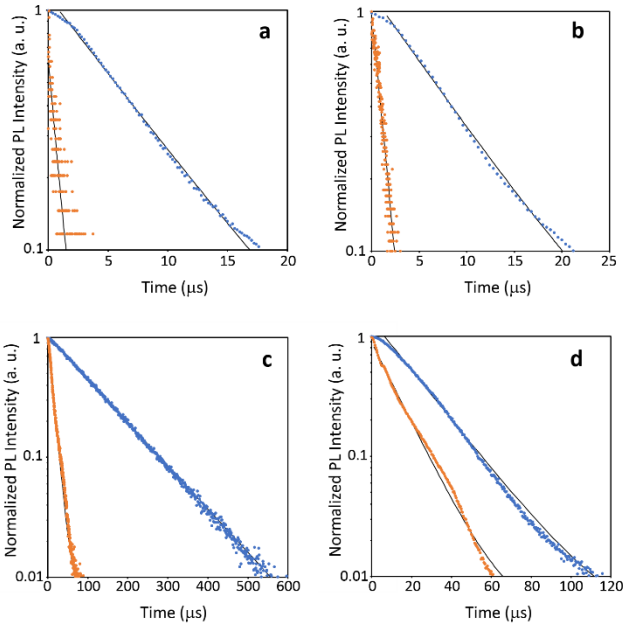

Figure 4. NIR decay dynamics of **[Ln(L₁)₃(H₂O)₂]** (orange dots) and **[Ln(L₁)₃(tppo)₂]** (blue dots) complexes excited in the ligand absorption band, with Ln a) Er^{3+} (λ_{em} = 1535 nm); b) Nd^{3+} (λ_{em} = 1060 nm); c) Sm^{3+} (λ_{em} = 950 nm); d) Yb^{3+} (λ_{em} = 982 nm). Solid black lines represent the best fit of the data.

The Ln emission decay dynamics in the NIR, shown in Figure 4 for the complexes with ligand L_1 and in Figure S32 in SI for the analogs with ligand L_2, are consistent with the observations made with steady-state measurements. The observed decay time constants τ_{obs} of all the complexes are significantly increased upon replacement of water molecules with tppo ligands, a summary can be found in Table 1. In particular, Er^{3+} and Sm^{3+} emission lifetimes increase by about one order of magnitude, whereas for Nd^{3+} a remarkable 8-fold lengthening is observed. As expected, these ions are the most sensitive to quenching by water, so it may appear not entirely surprising that the lifting of this deactivation channel leads to a remarkable improvement of the decay times. It is however worth noting that this improvement exceeds that expected for a simple removal of water molecules where the emitter sits within an environment rich of C-H deactivating groups (0.045 $Å^{-3}$ and 0.042 $Å^{-3}$, for **[Ln(L₁)₃(tppo)₂]** and **[Ln(L₂)₃(tppo)₂]**, respectively).[14c] As a matter of fact, the Er^{3+} and Nd^{3+} observed lifetimes are highly unusual in molecular complexes with organic ligands.[17b,19-24] Similar observations can be made for Yb^{3+} which unexpectedly displays a two-fold increase of the observed lifetime despite the fact this ion should in principle be significantly less sensitive to quenching by water since its single line emission at around 980 nm only justifies resonance with the third vibrational harmonic of H_2O stretching (whose fundamental modes are found at 3400 – 3700 cm^{-1}, see Figure S4 in SI) which is expected to be much weaker than the lower overtone. [9,13]

However, to achieve a full picture of the performances of the Ln emitters in such complexes it is also necessary to take into account their individual oscillator strength in the different coordination environments. The "natural" radiative lifetime τ_{rad}, i.e. the lifetime the emitter would have in the absence of any quenching phenomenon, is a parameter that strictly depends on the chemical surroundings (symmetry, degree of orbital mixing, vibrational coupling, ligand charge transfer states…) of the Ln ion.[26] It has been already discussed how the change in the coordination sphere on going from water to tppo containing complexes induces a modification of the spectral shapes of emission and absorption peaks pointing out the necessity to assess τ_{rad} for each individual molecular species. It is known that the determination of this parameter can be a rather difficult task requiring rather tedious calculations that can be subjected to large errors.[15] However, for the Ln ions whose absorption spectrum corresponding to the same transition giving rise to emission is known, the radiative lifetime can be retrieved from the absorption cross-section $\sigma_{Ln}(\lambda)$ though the Strickler-Berg equation (1):

$$\tau_{rad}^{-1} = 8\pi n^2 c \frac{1}{\langle\lambda^3\rangle} \frac{2J+1}{2J'+1} \int \frac{\sigma_{Ln}(\lambda)}{\lambda} d\lambda \qquad (1)$$

where *n* is the refractive index of the medium, *c* is the speed of light in vacuum and J and J' refer to the ground and excited state, respectively.

Lanthanide intrinsic emission quantum yields Φ_{Ln} can then be calculated through equation (2):

$$\Phi_{Ln} = \frac{\tau_{obs}}{\tau_{rad}} \quad (2)$$

The radiative lifetimes for Nd^{3+}, Er^{3+} and Yb^{3+} complexes have been experimentally determined using equation (1) from absorption spectra in $CDCl_3$ solution (~10^{-2} M, n = 1.445), see Figures S33-35 and Table S2 in SI. For solid state compounds, a correction for the refractive index of the medium (taken as n =1.517) [14c] has been applied, under the assumption that the coordination sphere of the complexes is preserved in the two phases, as suggested by ESI-mass data. In the case of Sm^{3+}, the absence of an absorption feature related to the excited $^4G_{5/2}$ level prevents applying the same method, so a literature value, retrieved from experimental absolute quantum yield and time-resolved data for a similar Sm^{3+} complex, was taken as reference. τ_{rad} and Φ_{Ln} values for the investigated complexes are given in Table 1.

Table 1. Observed lifetime, radiative lifetime and intrinsic quantum yield for the studied complexes measured in solid-state at room temperature.

Complex	τ_{obs} [μs]	Transition	τ_{rad} [ms]	Φ_{Ln} [%]
[Nd(L$_1$)$_3$(H$_2$O)$_2$]	1.15(0.02)	$^4F_{3/2} \rightarrow {}^4I_{11/2}$	0.77(0.08)	0.15(0.02)
[Nd(L$_1$)$_3$(tppo)$_2$]	8.96(0.07)	$^4F_{3/2} \rightarrow {}^4I_{11/2}$	0.87(0.09)	1.03(0.10)
[Nd(L$_2$)$_3$(H$_2$O)$_2$]	1.10(0.02)	$^4F_{3/2} \rightarrow {}^4I_{11/2}$	0.73(0.07)	0.15(0.02)
[Nd(L$_2$)$_3$(tppo)$_2$]	8.49(0.04)	$^4F_{3/2} \rightarrow {}^4I_{11/2}$	0.91(0.09)	0.94(0.11)
[Sm(L$_1$)$_3$(H$_2$O)$_2$]	12.61(0.3)	$^4G_{5/2} \rightarrow {}^6F_{5/2}$	29.8(0.3) [a]	0.04(0.01)
[Sm(L$_1$)$_3$(tppo)$_2$]	126.6(0.3)	$^4G_{5/2} \rightarrow {}^6F_{5/2}$	29.8(0.3) [a]	0.42(0.04)
[Sm(L$_2$)$_3$(H$_2$O)$_2$]	15.88(0.07)	$^4G_{5/2} \rightarrow {}^6F_{5/2}$	29.8(0.3) [a]	0.05(0.01)
[Sm(L$_2$)$_3$(tppo)$_2$]	132.95(0.33)	$^4G_{5/2} \rightarrow {}^6F_{5/2}$	29.8(0.3) [a]	0.45(0.04)
[Er(L$_1$)$_3$(H$_2$O)$_2$]	0.83(0.03)	$^4I_{13/2} \rightarrow {}^4I_{15/2}$	2.71(0.27)	0.03(0.01)
[Er(L$_1$)$_3$(tppo)$_2$]	7.50(0.04)	$^4I_{13/2} \rightarrow {}^4I_{15/2}$	4.37(0.44)	0.17(0.02)
[Er(L$_2$)$_3$(H$_2$O)$_2$]	0.68(0.04)	$^4I_{13/2} \rightarrow {}^4I_{15/2}$	1.88(0.19)	0.04(0.01)
[Er(L$_2$)$_3$(tppo)$_2$]	8.73(0.05)	$^4I_{13/2} \rightarrow {}^4I_{15/2}$	4.61(0.46)	0.19(0.02)
[Yb(L$_1$)$_3$(H$_2$O)$_2$]	12.74(0.07)	$^2F_{5/2} \rightarrow {}^2F_{7/2}$	0.44(0.04)	2.88(0.29)
[Yb(L$_1$)$_3$(tppo)$_2$]	24.78(0.24)	$^2F_{5/2} \rightarrow {}^2F_{7/2}$	0.38(0.04)	6.46(0.65)
[Yb(L$_2$)$_3$(H$_2$O)$_2$]	12.00(0.04)	$^2F_{5/2} \rightarrow {}^2F_{7/2}$	0.51(0.05)	2.35(0.24)
[Yb(L$_2$)$_3$(tppo)$_2$]	26.10(0.25)	$^2F_{5/2} \rightarrow {}^2F_{7/2}$	0.41(0.04)	6.33(0.63)

[a] Reference value taken from ref. 25 and appropriately corrected for the refractive index.

As it can be noticed from the reported data the radiative lifetimes of erbium and neodymium complexes change significantly upon replacement of coordinated water molecules with tppo ligands, which induce a lengthening in the values. This effect is more pronounced for Er^{3+}, whose radiative lifetime values in **[Er(L$_1$)$_3$(H$_2$O)$_2$]** and **[Er(L$_2$)$_3$(H$_2$O)$_2$]** fall in between two and three milliseconds range and almost double in **[Er(L$_1$)$_3$(tppo)$_2$]** and **[Er(L$_2$)$_3$(tppo)$_2$]** complexes to values around five milliseconds, in agreement with previous findings.[19a,b] An opposite trend is instead observed for the complexes of the strongest oscillator Yb^{3+} where the introduction of tppo moieties in place of water leads to a slight shortening of τ_{rad}. It is also interesting to note that the retrieved values, lying in the range 0.38 - 0.51 ms, are remarkably shorter than literature values usually comprised between 0.6 and 1.3 ms.[16a]

From the data in Table 1 it can be also noticed that the enhancement of the Er^{3+} observed lifetimes in tppo derivatives overcomes the increase of the radiative lifetime with respect to the water-containing analogs, leading to intrinsic quantum yields that are one order of magnitude higher and are highly unusual in coordination compounds.[17b,19-22] Similar considerations can be drawn for Nd^{3+},[16c,21bc,22-24] whereas for Yb^{3+},[21-23,27-28] the observed rather high quantum yields are mainly driven by the relatively high oscillator strength (short τ_{rad}) found for these complexes. Nonetheless, the quantum yield values for this ion display a two-fold increase up to a remarkable ~6.5% on going from **[Yb(L$_{1(2)}$)$_3$(H$_2$O)$_2$]** to **[Yb(L$_{1(2)}$)$_3$(tppo)$_2$]** which stems from the increase in the observed lifetimes.[27a,b]

These findings point out that the main reason behind the remarkable quantum yields observed in the **[Ln(L$_{1(2)}$)$_3$(tppo)$_2$]** complexes definitely lies in the significant reduction of emission quenching phenomena. Even in the light of the variations in the oscillator strength of the emitters in the different coordination environments, the observations made for the behavior in the emission dynamics still hold. In many cases the enhancement of the emission performances is beyond that expected from the sole removal of the vibrational deactivation channel due to water molecules, especially when considering the doubled number of C-

H quenchers upon the introduction of tppo units. These observations definitely claim for a deeper understanding of the factors governing quenching phenomena in NIR-emitting lanthanide complexes.

Vibrational quenching through Förster's resonance energy transfer model.

To achieve a more quantitative insight of the vibrational quenching occurring in the investigated β-diketonate compounds, we have implemented the Förster's model of resonance energy transfer on the basis of experimental structural and spectroscopic data for the whole series of sixteen water-containing and water-free complexes herein presented. According to the model, the energy transfer rate constant κ_{ET} from the energy donor (D) to a distribution of A_i acceptors in the surroundings of the emitter can be written as in equation (3):

$$\kappa_{ET} = \frac{1}{\tau_{ET}} = \kappa_D \sum_i \left(\frac{R_{0_i}}{R_{DA_i}}\right)^6 \quad (3)$$

where κ_D is the rate constant of the radiative decay of the donor in the absence of the acceptor, which, assuming that vibrational quenching is the sole relevant deactivation channel in these systems, can be taken as the radiative lifetime of the emitter, $\kappa_D = \kappa_{rad}$. $R_{DA,i}$ is the donor-acceptor distance and $R_{0,i}$ the Förster's radius, at which the energy transfer efficiency is 0.5. In turn, R_{0i} depends on the overlap integral *J* between the spectral emission of the donor $F_D(\lambda)$ normalized to unity and the absorption cross-section $\sigma_{Ai}(\lambda)$ of the A_i acceptor:

$${R_{0_i}}^6 = \frac{9K_i^2}{128\pi^5 n^4} \int F_D(\lambda)\sigma_{A_i}(\lambda)\lambda^4 d\lambda = \frac{9K_i^2}{128\pi^5 n^4} J \quad (4)$$

In equation (4) n is the refractive index of the medium and κ^2_i is a geometrical parameter that depends on the relative orientation of the donor and acceptor dipoles and can assume values in the range 0-4.[6]

In principle, the assessment of the rate constant of the vibrational deactivation implies the calculation of the individual κ^2_i parameters stemming from the contribution of all quenching sites in the proximity of the emitting ion, which is quite a cumbersome task requiring the detailed knowledge of the molecular structure and of transition dipole moments, which are not always available. For this reason in our approach we resorted to an approximation model by considering a continuous distribution of density of quenching sites ($\rho_A = N/4\pi R_{DA}^3$, where N is the number of quenchers) above the minimum R_{DA} distance, R_{DA}^{min},[8] where κ^2_i assumes the average value 2/3 and the experimental absorption cross-section of energy acceptors, namely CH and OH groups, results from the contribution of all quencher units, so that $\Sigma_i\sigma_{Ai}(\lambda) = \sigma_A(\lambda)$ (Figure 5). It is noted that $\sigma_A(\lambda)$ contains the information on the number N of quenching oscillators.

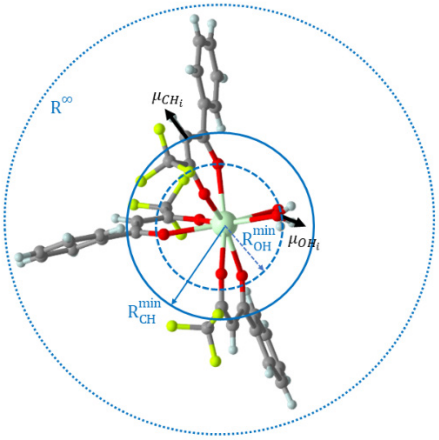

Figure 5. Representation of a water-containing β-diketonate molecular structure where the transition dipole moments of the *i*th CH and OH oscillators are depicted as black arrows and the circles delimit a continuous distribution of density of quenching sites above the minimum R_{CH}^{min} or R_{OH}^{min} distance from the lanthanide emitter, according to the described model.

Under these assumptions, the rate constant of the vibrational deactivation through CH and OH groups can be simply written as:

$$\kappa_{CH(OH)} = \kappa_{rad}\left(\frac{R_0}{R_{CH(OH)}^{min}}\right)^6 = \kappa_{rad}\left(R_{CH(OH)}^{min}\right)^{-6}\frac{3}{64\pi^5 n^4}J \quad (5)$$

where

$$J = \int F_D(\lambda)\sigma_{CH(OH)}(\lambda)\lambda^4 d\lambda \quad (6)$$

κ_{CH} and κ_{OH} can be calculated separately in the cases where water molecules are present in the first coordination sphere. The efficiency of the process ($\eta_{CH(OH)}$) is given by the following equation (7):

$$\eta_{CH(OH)} = \frac{1}{1+\frac{\kappa_{rad}}{\kappa_{CH(OH)}}} \quad (7)$$

while the predicted values for the intrinsic quantum yield can be retrieved by summing the rate constant for CH and OH deactivation:

$$\Phi_{Ln} = \frac{\kappa_{rad}}{\kappa_{rad}+\kappa_{CH}+\kappa_{OH}} \quad (8)$$

Overlap integrals were estimated by averaging the emission spectral density $F_{Ln}(\lambda)$ of the lanthanide emitters over the experimental absorption spectra of CH and OH groups in the NIR. A summary of spectral data in the NIR range is depicted in Figure 5 for the series of complexes with the L_1 ligand, while the corresponding spectra for the compounds with the L_2 ligand can be found in SI (Figure S36).

10.1002/chem.201904320

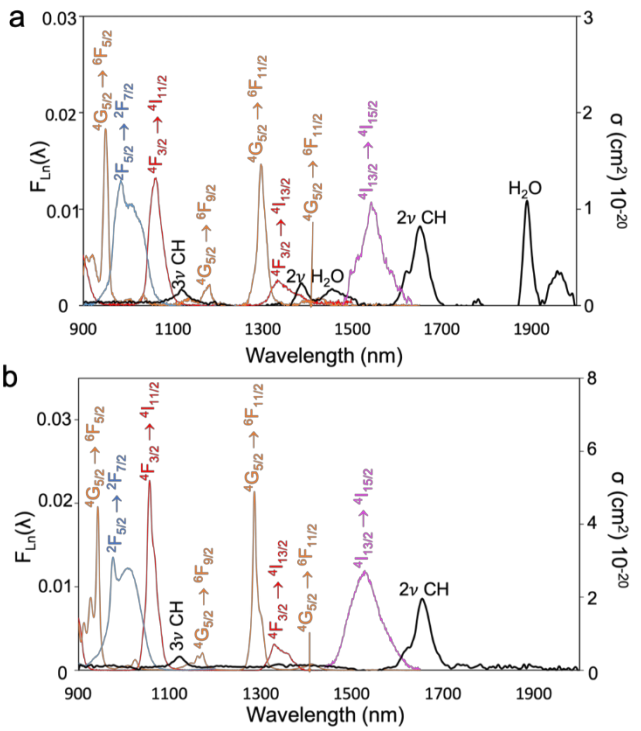

Figure 6. Normalized emission spectra of Ln^{3+} ions (Nd^{3+}, purple; Sm^{3+}, orange; Er^{3+}, pink; Yb^{3+} blue) and absorption cross-section (black) of vibrational overtones and combination bands of quenching groups in the NIR for **[Ln(L₁)₃(H₂O)₂]** (a) and **[Ln(L₁)₃(tppo)₂]** (b) compounds.

As evidenced in Figure 6, several absorption bands of vibrational overtones of CH and OH groups appear in the 900-2000 nm range. The second (2v CH) and third harmonics (3v CH) of the CH stretching mode around 1650 and 1130 nm are present in all spectra, whereas in the spectra of the water-containing compounds, the second overtone of OH stretching (2v OH) in the region around 1400 nm and the combination of OH stretching and H_2O bending ($av_1+v_2+bv_3$, with v_1 symmetric, v_2 antisymmetric stretching and v_3 bending) close to 1900 nm are visible. Both these spectral features consist of a set of a sharp band on the higher energy side related to free OH groups and a broader one at lower energy attributable to OH groups sharing hydrogen bonding in agreement with the sequence of peaks in the FT-IR spectra of the compounds (see SI). In order to disentangle the contribution of quenchers present in the molecular complex from the solvent background, diffuse absorbance (DA) spectra of solid-state samples, appropriately rescaled in terms of absorption cross-section (see SI and Figures S33-S35), were used. In particular, DA spectra of the Nd^{3+} derivatives were taken into consideration since no lanthanide absorption line overlaps with the vibrational bands of the quenchers in the 900-2000 nm spectral region. It has to be pointed out that the model and the following discussion are solely referred to the effect of CH and OH groups in quenching phenomena and other deactivation channels or multi-phonon relaxations are not considered herein (see SI for details). A summary of the calculated main parameters for this model are reported in Table 2.

Table 2. Förster's energy transfer model parameters.

Complex		J x 10^3 (nm^6)	R_{DA} (min) [nm]	$\kappa_{CH(OH)}$ (ms^{-1})	η_{CH} or η_{OH} [%]	Predicted Φ_{Ln} [%]
[Nd(L₁)₃(H₂O)₂]	CH	10.2(1.0)	0.408(2)	78(18)	98.52(9.85)	0.03
	OH	33.5(3.5)	0.263(5)	3600(890)	99.97(10.00)	
[Nd(L₁)₃(tppo)₂]		19.2(1.9)	0.435(4)	90(11)	98.85(9.88)	1.15
[Nd(L₂)₃(H₂O)₂]	CH	10.8(1.1)	0.413(4)	82(19)	98.52(9.86)	0.03
	OH	36.0(3.6)	0.267(3)	3744(911)	99.97(9.99)	
[Nd(L₂)₃(tppo)₂]		17.8(1.8)	0.432(3)	83(20)	98.81(9.89)	1.19
[Sm(L₁)₃(H₂O)₂]	CH	6.7(0.7)	0.405(2)	1.70(0.40)	97.87(9.79)	0.08
	OH	11.5(1.2)	0.260(5)	42(11)	99.91(9.99)	
[Sm(L₁)₃(tppo)₂]		17.3(1.7)	0.432(3)	3.00(0.73)	98.78(9.88)	1.22
[Sm(L₂)₃(H₂O)₂]	CH	6.1(0.6)	0.422(4)	1.21(0.29)	97.02(9.70)	0.11
	OH	12.9(1.3)	0.267(3)	33(8)	99.89(9.98)	

[Sm(L$_2$)$_3$(tppo)$_2$]		16.7(1.7)	0.429(3)	3.02(0.72)	98.79(9.89)	1.21
[Er(L$_1$)$_3$(H$_2$O)$_2$]	CH	143.0(14.3)	0.398(2)	368(88)	99.91(9.99)	0.01
	OH	55.0(5.5)	0.252(5)	2161(548)	99.98(10.00)	
[Er(L$_1$)$_3$(tppo)$_2$]		197.0(19.7)	0.424(4)	213(52)	99.90(9.99)	0.10
[Er(L$_2$)$_3$(H$_2$O)$_2$]	CH	145.5(14).6	0.402(4)	500(121)	99.90(9.99)	0.01
	OH	52.8(5.3)	0.257(3)	2700(660)	99.98(10.00)	
[Er(L$_2$)$_3$(tppo)$_2$]		211.4(21.1)	0.421(3)	226(54)	99.91(9.99)	0.09
[Yb(L$_1$)$_3$(H$_2$O)$_2$]		2.3(0.2)	0.396(2)	37(9)	94.78(9.48)	5.22
[Yb(L$_1$)$_3$(tppo)$_2$]		6.6(0.7)	0.422(4)	83(20)	97.24(9.72)	2.76
[Yb(L$_2$)$_3$(H$_2$O)$_2$]		2.1(0.2)	0.401(4)	27(7)	93.89(9.39)	6.11
[Yb(L$_2$)$_3$(tppo)$_2$]		6.3(0.6)	0.419(3)	77(18)	97.23(9.73)	2.77

As can be seen from the comparison of data in Table 2 and 1 and from, predictions on the emission efficiency of lanthanide ions retrieved from the model are satisfactorily in agreement with the 'real values' obtained from time-resolved and steady state measurements (Figure S37).

A closer analysis of the data reported in Table 2 allows disentangling the contribution of the different parameters involved in the vibrational quenching in NIR-emitting lanthanide complexes.

Er^{3+} complexes.

Among the studied emitters, Er^{3+} is indeed the most affected by vibrational deactivation as, besides the long wavelengths spectral region involved (Eq 6), large overlap integrals result from the resonance with the first overtones of CH and OH stretching modes as also evident from Figure 6. The contribution of these two oscillators in **[Er(L$_{1(2)}$)$_3$(H$_2$O)$_2$]** was calculated separately and the overall quenching effect results from the synergy of both oscillators according to Equation (7). As expected, the presence of highly resonant water molecules at short distance from the emitter accounts for the quantum yield values well below 0.1% found for the **[Er(L$_{1(2)}$)$_3$(H$_2$O)$_2$]** compounds. It is worth noting that the influence of higher energy oscillating free OH groups is practically negligible with respect to hydrogen bonded ones whose overtone is more resonant with Er^{3+} emission at 1.5 μm (Figure 3a). The replacement of these bonded water molecules with tppo ligands leads to a substantial increase in the observed lifetimes and intrinsic quantum yields. In **[Er(L$_{1(2)}$)$_3$(tppo)$_2$]** only the contribution of the second harmonic (2v CH) of vibrational CH stretching can be identified, whereas the influence of the third harmonic (3v CH) to the depopulation of the superior $^4I_{11/2}$ level of Er^{3+} (which feeds the lower lying $^4I_{13/2}$ state) can be considered negligible. The quenching effect of the CH oscillators remains strong but the effect of the two-fold added amount of CH groups in the proximity of the emitter that have replaced the OH oscillators is lower than expected for a direct proportionality with the number of quenching sites. This behavior can be explained by taking into consideration the parameters reported in Table 2 and the spectral overlap in Figure 6. In fact, the coordination of the sterically cumbersome tppo induces a significant lengthening (~0.2 Å) of the distance between the metal emitter and the nearest CH group in the α- position of the β-diketonate ligand while the relatively poor resonance of Er^{3+} emission with the CH absorption band only causes a small (~25%) increase in the value of the overlap integral. As a result, the efficiency of the CH deactivation channel is approximately similar in all complexes and the use of a fully fluorinated tppo ligand to displace coordinated water molecules would only lead to a small enhancement (~0.04%) of the emission quantum yield. From these findings, it can be inferred that the rate constant for the vibrational deactivation of Er^{3+} emission by CH groups has a weak dependence on the total number of quenching sites whereas the donor-acceptor distance takes on a much higher importance. This is in line with the previous observation that the nearest neighbor CH oscillators are the most relevant[13] in quenching Er^{3+} emission and it explains the longer lifetimes observed in the tppo derivatives with respect to those typical for complexes bearing a similar number of CH groups and even highly fluorinated analogous compounds.[20b]

Nd^{3+} complexes.

Similar conclusions can be drawn for the Nd^{3+} derivatives where vibrational quenching phenomena arise mainly from the resonance with the first overtone of OH stretching (2v OH) in the 1300-1400 nm range **[Nd(L$_{1(2)}$)$_3$(H$_2$O)$_2$]** and the third harmonic of CH vibration (3v CH) at 1050-1150 nm (**[Nd(L$_{1(2)}$)$_3$(H$_2$O)$_2$]** and **[Nd(L$_{1(2)}$)$_3$(tppo)$_2$]**). Both these two deactivation channels contribute to the depopulation of the excited $^4F_{3/2}$ level giving rise to the emission bands at 1064 and 1340 nm in the water containing complexes. On replacement of water molecules in the first coordination sphere in **[Nd(L$_{1(2)}$)$_3$(tppo)$_2$]** the Nd^{3+} observed lifetimes and quantum yields increase to values exceeding those typical for CH-containing complexes, similarly to what observed

in the Er^{3+} derivatives.[22] In this case, beside the increased distance between the emitter and the nearest neighbor CH group, the significant change in shape of the Nd^{3+} $^4F_{3/2} \rightarrow {}^4I_{11/2}$ emission band as a consequence of the change in local symmetry upon coordination with the tppo ligands limits the increase in the overlap integral value expected for a doubled amount of CH groups (Figure 6 and Figure S38a). This explains the relatively long lifetimes observed in the **$[Nd(L_{1(2)})_3(tppo)_2]$** derivatives beyond the increase in the radiative lifetimes.

Sm^{3+} complexes.

The β-diketonate ligand photosensitization allows multiple emission lines from Sm^{3+} in the NIR, including an intense band in the second telecommunication window at 1300 nm and a weaker one at 1400 nm. The samarium emission bands that are submitted to quenching are at 1030 nm, 1170 nm and 1400 nm, all originating from the same excited level $^4G_{5/2}$, where the first two emission bands are in resonance with the third vibrational harmonic of CH oscillators and the latter falls in the overlap region with the second vibrational harmonic of OH oscillators (see Figure S36 a and b in SI). In **$[Sm(L_{1(2)})_3(H_2O)_2]$** the overall vibrational quenching efficiency arises from all the above contributions where the effectiveness of CH oscillators is significantly lower than that of OH oscillators in view of the higher overlap integral and the shorter distance of the directly coordinated water molecules. It is then not surprising that upon removal of the vibrational deactivation channels due to water in **$[Sm(L_{1(2)})_3(tppo)_2]$** complexes, the observed lifetimes and quantum yields increase by about one order of magnitude.[16d,24c,25,26] However, a closer look at the data in Table 2 reveals that the efficiency of vibrational quenching by CH oscillators increases by about 1%. In this case the influence of the increased number of quenchers is considerably more accentuated with respect to that observed for Er^{3+} and Nd^{3+} derivatives and originates mainly from the increased spectral overlap with the CH overtone, despite the change in the emission spectral shape on going from water-containing to water-free complexes slightly mitigates this effect, as also observed in the Nd^{3+} derivatives (Figure S38b).

Additionally, it should be remarked that, on the basis of the model, the literature value of 27 ms of the Sm^{3+} radiative lifetime seems overestimated whereas a value around 13 ms would yield decay rate constants ($\kappa_{CH} + \kappa_{OH}$) closer to the observed ones ($\kappa_{obs} = 1/\tau_{obs}$) for the whole set of complexes, under the assumption that no other deactivation channel is present other than vibrational quenching. This would imply that the intrinsic quantum yields reported in Table 1 might be underestimated approximately by a factor of two. These observations point out that the Förster's model may be also used as an indirect tool to assess the oscillator strength of lanthanide emitters.

Yb^{3+} complexes.

While the general trend of enhanced emission performances upon water displacement can be rather easily explained in Er^{3+}, Nd^{3+} and Sm^{3+} complexes, the two-fold increase in the emission lifetime and quantum yield observed for the Yb^{3+} derivatives requires more consideration. Experimental evidence from spectral data suggests that the only relevant quenching pathway in this case stems from the resonance with the 3v CH overtone (see Figure S36 a and b in SI). Implementation of the Förster's model on this basis yields predicted quantum yields that are in opposite trend with the observed values and derive from an increased overlap integral whose effect is not offset by the donor-acceptor distance lengthening on going from water-containing to tppo derivatives. Neglecting deviations that could derive from the experimental evaluation of the radiative lifetime of the strongest oscillator out of the investigated set of lanthanides and the relatively large errors associated with the small values of the overlap integrals due to the weak resonance, we can suggest that the discrepancy found for the **$[Yb(L_{1(2)})_3(H_2O)_2]$** complexes may originate from the overlap with the absorption band of the third harmonic of the OH stretching vibration (3v OH) which can be predicted to lie right beneath the Yb^{3+} emission line at 1 μm. It is possible that this band is broadened to a point where it falls below the signal-to-noise ratio in the experimental DA spectra thus becoming undetectable. In the case of the Er^{3+}, Nd^{3+} and Sm^{3+} the influence of this resonance would be negligible with respect to that with the OH harmonic of lower quantum (2v OH) but in Yb^{3+} it may explain the lowering in the observed quantum yields with respect to the expected values. However, these considerations cannot account for the significant underestimation of the quantum yields (and lifetimes) with respect to the observed ones in **$[Yb(L_{1(2)})_3(tppo)_2]$** complexes. We can only speculate that the Förster's model in the continuous density approximation fails in describing the dependence of the distance of the emitter to the nearest neighbor oscillator where the donor-acceptor resonance condition is weak as in the case of Yb^{3+} with CH oscillators. It is however noted that an increase in the donor-acceptor separation to 7.5 Å would dramatically affect the emission quantum yield to values around 50%.

Conclusions

Sixteen new lanthanide tris β-diketonate complexes with two different asymmetrical ligands (L_1 and L_2) bearing a trifluoromethane and a hydrogenated phenyl group substituted with a chlorine atom in the para-position in L_2 have been reported. The as-synthesized complexes bear two water/solvent molecules in the first coordination sphere that can be easily replaced by neutral tppo monodentate units to afford OH-free compounds. Five complexes were structurally characterized with single crystal X-ray diffraction analysis and their molecular structures were described. All the complexes show NIR emission upon ligand excitation which is considerably boosted upon water removal by replacement with tppo units. Despite the increased number of CH quenching groups, the emission lifetimes of OH-free compounds are lengthened, up to values that are unusually long for Er^{3+} (~8 μs) and Nd^{3+} (~9 μs) hydrogenated complexes while Yb^{3+} complexes display remarkable intrinsic quantum yields up to ~6.5% benefitting from short radiative lifetimes in the range 0.4-0.5 ms. Novel detailed insights on the NIR emission of Sm^{3+} complexes have been provided, showing that an increase in the emission lifetime of about one order of magnitude, from ~13-16 to ~130 μs, can be achieved upon removal of water molecules directly coordinated to the metal.

10.1002/chem.201904320

An extended and detailed experimental systematic study has been carried out on the factors governing vibrational quenching in NIR-emitting Nd^{3+}, Sm^{3+}, Er^{3+} and Yb^{3+} complexes by implementing the Förster's model of resonance energy transfer on the basis of structural and spectroscopic data. It has been shown that the efficiency of vibrational quenching by OH and CH groups can be modeled with good accuracy, down to deviations well below 1% from experimental values, by considering a continuous spatial distribution of quenching sites located above the minimum distance of the nearest neighbor OH or CH quencher from the emitter. The results obtained from these model calculations have allowed to explain the observed rather long emission lifetimes that are highly unexpected for complexes bearing a large number of CH groups (>0.04 $Å^{-3}$) sitting in the immediate surroundings of the metal emitter. It has been unveiled that two factors can have a crucial role in governing the effectiveness of CH vibrational deactivation beyond the number of quenching sites. These are the increased distance of the nearest neighbor methine group of the β-diketonate ligand upon insertion of the sterically cumbersome tppo unit, and the change in the lanthanide spectral emission shape as a consequence of the variation in the local coordination symmetry. In particular, for Er^{3+}, the former parameter takes on more importance over the limited increase in the spectral overlap with the first vibrational CH overtone, pointing out that emission is definitely more sensitive to the spatial separation than to the total amount of quenchers in the surroundings. Similar considerations can be made for Yb^{3+} and, for both these ions, this originates from the rather weak spectral overlap between the lanthanide emission and the absorption peak of the involved CH spectral overtone. In the case of Nd^{3+}, the significant narrowing of the emission band at 1064 nm in the tppo derivatives with respect to the water-containing complexes, limits to a great extent the effect of the increase of CH absorption on the spectral overlap and hence the sensitivity to the increased number of quenchers, justifying the observed unusual rather long-lived emission. The same mitigating effect is observed in Sm^{3+} complexes, although the strong resonance between Sm^{3+} emission and the CH second overtone makes this ion highly sensitive to vibrational quenching. As additional remark, it is worth pointing out that the application of the Förster's model/theory for vibrational quenching is a valuable and relatively simple alternative route to assess the radiative lifetime of Sm^{3+}, which is usually retrieved through cumbersome calculations.

The conclusions herein drawn from the detailed analysis of the quenching effects of OH and CH groups in the framework of the Förster's theory provide useful general guidelines for the design of NIR emitting lanthanide complexes with enhanced properties while still resorting to facile, accessible and cheap syntheses. In fact, whereas fully dehydrogenated compounds, where vibrational quenching is entirely suppressed, indeed represent the best performing materials achievable, it has been herein shown that, in several cases, remarkably long-lived emission and relatively high quantum yields can still be obtained without the use of expensive and difficultly prepared perfluorinated or perdeuterated ligands. These results can open new perspectives for the development of lanthanide complexes as NIR emitters for practical applications.

Experimental Section

Materials. The lanthanide chloride hydrates (99.9%) were purchased from Sigma Aldrich ($NdCl_3·6H_2O$, $SmCl_3·6H_2O$, $ErCl_3·6H_2O$, $YbCl_3·6H_2O$). 4,4,4-trifluoro-1-phenyl-1,3-butadione (Hbfa) 99%, chloroform-d and DMSO-d^6 for NMR (99.8% atom D) were purchased from Acros Organics, 4,4,4-trifluoro-1-(4-chlorophenyl)-1,3-butadione, 98% was purchased from TCI Europe, triphenylphosphine oxide was purchased from Sigma Aldrich, methanol (laboratory grade, 100%), acetonitrile (analytical grade) and NaOH were purchased from Fisher Scientific. All chemicals were used without further purification.

Synthesis of $[Ln(L_1)_3(H_2O)_2]$ and $[Ln(L_2)_3(H_2O)_2]$. Synthesis procedure was similar for both complexes except for the used β-diketonate ligand. In 5 mL of methanol an appropriate amount of ligand **L_1** or **L_2** (0.9 mmol) was dissolved and deprotonated with an equivalent molar amount of sodium hydroxide (0.9 mmol) and left for an hour to stir. A methanol solution of $LnCl_3·6H_2O$ was prepared by dissolving of $LnCl_3·6H_2O$ (Ln^{3+} = Nd^{3+}, Sm^{3+}, Er^{3+} and Yb^{3+}) (0.3 mmol) in 3 mL of methanol. After an hour the solution of $LnCl_3·6H_2O$ in methanol was added dropwise to the solution of the sodium salt and the mixture was left to stir for 24h at room temperature. When 24h passed the stirring was stopped and the mixture was left to slowly evaporate for 72h during which crystals were formed. The obtained crystals were filtered off and washed with distilled water and left to dry in air for one day. Then the product was recrystallized by slow evaporation from a methanolic solution (methanol with a few drops of water), yielding crystals suitable for single crystal X-ray diffraction analysis (also used for further analysis) for $[Ln(L_1)_3(H_2O)_2]$ complexes. For the $[Ln(L_2)_3(H_2O)_2]$ complexes this mixture of solvent did not give crystals suitable for single crystal X-ray diffraction, and it was slightly modified by adding acetonitrile to a methanolic solution to afford single crystals which could be structurally investigated.

$[Nd(L_1)_3(H_2O)_2]$: Elemental analysis (%) calculated for $C_{30}H_{22}F_9O_8Nd$ (825.73): C 43,64, H 2,69; Found: C 42,89 , H 2.59. FT-IR (KBr) ν (cm^{-1}): 3657 (O-H st, free), 3462 (O-H st, H-bonded), 3251, 3143 (C-O, enol beyond the range), 3062 (ar C-H st), 2913, 2774, 2715, 2590 (C-H, Fermi resonance), 2428, 2388, 2331, 2271, 2225, 2131 (aromatic overtone), 2038, 1972, 1910, 1820 (comb, aromatic), 1777 (C=O st, keto form), 1563, 1524, 1455 (ar C-C st), 1384, 1307 (C-F st, CF_3), 1245, 1186, 1139 (C-F st, CF_3 and ar C-H δ ip), 1081, 1014 (ar C-H δ ip), 944 (C-H δ oop), 808 (ar C-C γ), 781, 711 (C-F δ, CF_3, C-H δ oop and ar C-C γ). ESI-MS (positive mode, +); m/z: 827.15 $[M+H]^+$, 809.83 $[(M-H_2O)+H]^+$, 791.52 $[(M-2H_2O)+H]^+$. Isotope used for calculation is ^{145}Nd.

$[Sm(L_1)_3(H_2O)_2]$: Elemental analysis (%) calculated for $C_{30}H_{22}F_9O_8Sm$ (831.84): C 43.32, H 2.67; Found: C 43.13, H 2.58. FT-IR (KBr) ν_{max} (cm^{-1}): 3657 (O-H st, free), 3466 (O-H st, H-bonded), 3256, 3150 (C-O, enol beyond the range), 3062 (ar C-H st), 2917, 2766, 2719, 2595 (C-H, Fermi resonance), 2431, 2381, 2330, 2271, 2225, 2131 (aromatic overtone), 2042, 1972, 1910, 1824 (comb, aromatic), 1774 (C=O st, keto form), 1567, 1529, 1462 (ar C-C st), 1384, 1310 (C-F st, CF_3), 1248, 1190, 1143 (C-F st, CF_3 and ar C-H δ ip), 1073, 1023 (ar C-H δ ip), 941 (C-H δ oop), 809 (ar C-C γ), 785, 711 (C-F δ, CF_3, C-H δ oop and ar C-C γ). ESI-MS (positive mode, +); m/z: 834.12 $[M+H]^+$, 816.75 $[(M-H_2O)+H]^+$, 798.73 $[(M-2H_2O)+H]^+$. Isotope used for calculation is ^{155}Sm.

$[Er(L_1)_3(H_2O)_2]$: Elemental analysis (%) calculated for $C_{30}H_{22}F_9O_8Er$ (848.74): C 42.45, H 2.61; Found: C 42.36, H 2.54. FT-IR (KBr) ν_{max} (cm^{-1}): 3657 (O-H st, free), 3466 (O-H st, H-bonded), 3256, 3150 (C-O, enol beyond the range), 3062 (ar C-H st), 2921, 2769, 2719, 2595 (C-H, Fermi resonance), 2428, 2384, 2330, 2271, 2225, 2135 (aromatic overtone), 2042, 1972, 1910, 1824 (comb, aromatic), 1774 (C=O st, keto form), 1567,

1529, 1462 (ar C-C st), 1384, 1310 (C-F st, CF_3), 1248, 1190, 1147 (C-F st, CF_3 and ar C-H δ ip), 1081, 1023 (ar C-H δ ip), 945 (C-H δ oop), 809 (ar C-C γ), 770, 711 (C-F δ, CF_3, C-H δ oop and ar C-C γ). ESI-MS (positive mode, +); m/z: 850.76 $[M+H]^+$, 832.10 $[(M-H_2O)+H]^+$, 814.49 $[(M-2H_2O)+H]^+$. Isotope used for calculation is ^{167}Er.

[Yb(L$_1$)$_3$(H$_2$O)$_2$]: Elemental analysis (%) calculated for $C_{30}H_{22}F_9O_8Yb$ (854.54): C 42.17, H 2.60; Found: C 41.79, H 2.65. FT-IR (KBr) ν_{max} (cm^{-1}): 3657 (O-H st, free), 3470 (O-H st, H-bonded), 3256, 3151 (C-O, enol beyond the range), 3062 (ar C-H st), 2922, 2770, 2598 (C-H, Fermi resonance), 2428, 2381, 2326, 2271, 2225, 2135 (aromatic overtone), 2046, 1972, 1905, 1820 (comb, aromatic), 1777 (C=O st, keto form), 1567, 1525, 1462 (ar C-C st), 1381, 1310 (C-F st, CF_3), 1248, 1190, 1147 (C-F st, CF_3 and ar C-H δ ip), 1081, 1023 (ar C-H δ ip), 941 (C-H δ oop), 809 (ar C-C γ), 770, 711 (C-F δ, CF_3, C-H δ oop and ar C-C γ). ESI-MS (positive mode, +); m/z: 856.96 $[M+H]^+$, 838.95 $[(M-H_2O)+H]^+$, 820.10 $[(M-2H_2O)+H]^+$. Isotope used for calculation is ^{175}Yb.

[Nd(L$_2$)$_3$(H$_2$O)$_2$]: Elemental analysis (%) calculated for $C_{30}H_{19}Cl_3F_9O_8Nd$ (929.05): C 38.78, H 2.06; Found: C 37.86, H 2.01. FT-IR (KBr) ν_{max} (cm^{-1}): 3649 (O-H st, free), 3450 (O-H st, H-bonded), 3241, 3155 (C-O, enol beyond the range), 3065 (ar C-H st), 2879, 2832, 2762, 2676, 2587 (C-H, Fermi resonance), 2501, 2381, 2334, 2287, 2221, 2128 (aromatic overtone), 2046, 2003, 1914, 1793 (comb, aromatic), 1727, 1680 (C=O st, keto form), 1602, 1572 1529, 1478 (ar C-C st), 1369, 1291 (C-F st, CF_3), 1248, 1186, 1143 (C-F st, CF_3 and ar C-H δ ip), 1097, 1011 (ar C-H δ ip), 945 (C-H δ oop), 830 (ar C-C γ and C-Cl st), 797, 743 (C-F δ, CF_3, C-H δ oop, ar C-C γ and C-Cl st), 661 (C-Cl st). ESI-MS (positive mode, +); m/z: 931.77 $[M+H]^+$, 913.07 $[(M-H_2O)+H]^+$, 895.79 $[(M-2H_2O)+H]^+$. Isotope used for calculation is ^{145}Nd.

[Sm(L$_2$)$_3$(H$_2$O)$_2$]: Elemental analysis (%) calculated for $C_{30}H_{19}Cl_3F_9O_8Sm$ (935.17): C 38.53, H 2.05; Found: C 38.25, H 1.97. FT-IR (KBr) ν_{max} (cm^{-1}): 3653 (O-H st, free), 3450 (O-H st, H-bonded), 3248, 3155 (C-O, enol beyond the range), 3073 (ar C-H st), 2925, 2875, 2832, 2766, 2592 (C-H, Fermi resonance), 2502, 2381, 2376, 2283, 2221, 2124 (aromatic overtone), 2042, 2011, 1914, 1793 (comb, aromatic), 1727, 1684 (C=O st, keto form), 1598, 1572 1532, 1481 (ar C-C st), 1400, 1295 (C-F st, CF_3), 1248, 1186, 1143 (C-F st, CF_3 and ar C-H δ ip), 1097, 1011 (ar C-H δ ip), 945 (C-H δ oop), 844 (ar C-C γ and C-Cl st), 797, 743 (C-F δ, CF_3, C-H δ oop, ar C-C γ and C-Cl st), 661 (C-Cl st). ESI-MS (positive mode, +); m/z: 937.26 $[M+H]^+$, 919.03 $[(M-H_2O)+H]^+$, 901.91$[(M-2H_2O)+H]^+$. Isotope used for calculation is ^{155}Sm.

[Er(L$_2$)$_3$(H$_2$O)$_2$]: Elemental analysis (%) calculated for $C_{30}H_{19}Cl_3F_9O_8Er$ (952.01): C 37.85, H 2.01; Found: C 37.47, H 1.99. FT-IR (KBr) ν_{max} (cm^{-1}): 3653 (O-H st, free), 3431 (O-H st, H-bonded), 3229, 3155 (C-O, enol beyond the range), 3073 (ar C-H st), 2922, 2882, 2832, 2766, 2591 (C-H, Fermi resonance), 2502, 2381, 2376, 2326, 2283, 2221, 2124 (aromatic overtone), 2042, 2011, 1914, 1793 (comb, aromatic), 1723, 1684 (C=O st, keto form), 1598, 1572 1532, 1481 (ar C-C st), 1400, 1295 (C-F st, CF_3), 1248, 1186, 1143 (C-F st, CF_3 and ar C-H δ ip), 1097, 1011 (ar C-H δ ip), 945 (C-H δ oop), 844 (ar C-C γ and C-Cl st), 797, 743 (C-F δ, CF_3, C-H δ oop, ar C-C γ and C-Cl st), 661 (C-Cl st). ESI-MS (positive mode, +); m/z: 954.86 $[M+H]^+$, 936.63 $[(M-H_2O)+H]^+$, 918.87 $[(M-2H_2O)+H]^+$. Isotope used for calculation is ^{167}Er.

[Yb(L$_2$)$_3$(H$_2$O)$_2$]: Elemental analysis (%) calculated for $C_{30}H_{19}Cl_3F_9O_8Yb$ (957.86): C 37.62, H 2.00; Found: C 36.28, H 2.14. FT-IR (KBr) ν_{max} (cm^{-1}): 3653 (O-H st, free), 3423 (O-H st, H-bonded), 3248, 3155 (C-O, enol beyond the range), 3073 (ar C-H st), 2917, 2883, 2836, 2762, 2595 (C-H, Fermi resonance), 2501, 2385, 2326, 2283, 2283, 2132 (aromatic overtone), 2042, 2011, 1914, 1789 (comb, aromatic), 1727, 1680 (C=O st, keto form), 1603, 1567 1532, 1478 (ar C-C st), 1396, 1295 (C-F st, CF_3), 1252, 1186, 1143 (C-F st, CF_3 and ar C-H δ ip), 1093, 1011 (ar C-H δ ip), 941 (C-H δ oop), 844 (ar C-C γ and C-Cl st), 793, 739 (C-F δ, CF_3, C-H δ oop, ar C-C γ and C-Cl st), 665 (C-Cl st). ESI-MS (positive mode, +); m/z: 958.91 $[M+H]^+$, 940.76 $[(M-H_2O)+H]^+$, 922.89 $[(M-2H_2O)+H]^+$. Isotope used for calculation is ^{175}Yb.

Synthesis of [Ln(L$_1$)$_3$(tppo)$_2$] and [Ln(L$_2$)$_3$(tppo)$_2$]. The synthesis procedure was the same for both types of complexes, the only difference being in the starting complex. Tppo (0.2 mmol) was dissolved in 2 mL of methanol. A methanol solution of [Ln(L$_1$)$_3$(H$_2$O)$_2$] or [Ln(L$_2$)$_3$(H$_2$O)$_2$] (0.1 mmol) was added dropwise to the tppo solution and was left to stir for 1h. After 1h the solution was left to crystallize by slow evaporation. After 48h crystals suitable for single crystal X-ray diffraction analysis were formed and then collected from the mother liquor and left to dry in air.

[Nd(L$_1$)$_3$(tppo)$_2$]: Elemental analysis (%) calculated for $C_{66}H_{48}F_9P_2O_8Nd$ (1346.28): C 58.88, H 3.59; Found: C 58.68, H 3.53. FT-IR (KBr) ν_{max} (cm^{-1}): 3252, 3151 (C-O, enol beyond the range), 3062 (ar C-H st), 2956, 2769, 2715, 2595 (C-H, Fermi resonance), 2470, 2419, 2330, 2252, 2120 (aromatic overtone), 2034, 1968, 1902, 1816 (comb, aromatic), 1770 (C=O st, keto form), 1626, 1575, 1525, 1474 (ar C-C st), 1384, 1307 (C-F st, CF_3), 1284 (P=O st), 1240, 1183, 1140 (C-F st, CF_3, ar C-H δ ip and R_3P=O st), 1069, 1027 (ar C-H δ ip and R_3P=O st), 995 (R_3P=O st), 937 (C-H δ oop and R_3P=O st), 844, 801 (ar C-C γ and P-C st), 754, 696 (C-F δ, CF_3, C-H δ oop and ar C-C γ). ESI-MS (positive mode, +); m/z: 1410.26 $[M+ACN+Na]^+$, 1132.14 $[(M-TPPO)+ACN+Na]^+$, 557.39 $[2TPPO+H]^+$, 279.08 $[TPPO+H]^+$. Isotope used for calculation is ^{145}Nd.

[Sm(L$_1$)$_3$(tppo)$_2$]: Elemental analysis (%) calculated for $C_{66}H_{48}F_9P_2O_8Sm$ (1352.40): C 58.62, H 3.58; Found: C 58.22, H 3.49. FT-IR (KBr) ν_{max} (cm^{-1}): 3252, 3151 (C-O, enol beyond the range), 3062 (ar C-H st), 2956, 2774, 2711, 2595 (C-H, Fermi resonance), 2470, 2419, 2326, 2252, 2120 (aromatic overtone), 2034, 1968, 1902, 1816 (comb, aromatic), 1770 (C=O st, keto form), 1617, 1572, 1525, 1478, 1439 (ar C-C st), 1381, 1307 (C-F st, CF_3), 1284 (P=O st), 1241, 1183, 1132 (C-F st, CF_3, ar C-H δ ip and R_3P=O st), 1073, 1026 (ar C-H δ ip and R_3P=O st), 992 (R_3P=O st), 937 (C-H δ oop and R_3P=O st), 844, 801 (ar C-C γ and P-C st), 754, 700 (C-F δ, CF_3, C-H δ oop and ar C-C γ). ESI-MS (positive mode +), m/z: 1416.35 $[M+ACN+Na]^+$, 1138.20 $[(M-TPPO)+ACN+Na]^+$, 557.17 $[2TPPO+H]^+$, 279.29 $[TPPO+H]^+$. Isotope used for calculation is ^{145}Sm.

[Er(L$_1$)$_3$(tppo)$_2$]: Elemental analysis (%) calculated for $C_{66}H_{48}F_9P_2O_8Er$ (1369.29): C 57.89, H 3.53; Found: 56.58, H 3.32. FT-IR (KBr) ν_{max} (cm^{-1}): 3256, 3151 (C-O, enol beyond the range), 3062 (ar C-H st), 2960, 2774, 2715, 2595 (C-H, Fermi resonance), 2474, 2419, 2326, 2252, 2120 (aromatic overtone), 2034, 1968, 1906, 1820 (comb, aromatic), 1774 (C=O st, keto form), 1617, 1579, 1521, 1478, 1443 (ar C-C st), 1381, 1310 (C-F st, CF_3), 1288 (P=O st), 1241, 1183, 1136 (C-F st, CF_3, ar C-H δ ip and R_3P=O st), 1085, 1027 (ar C-H δ ip and R_3P=O st), 995 (R_3P=O st), 937 (C-H δ oop and R_3P=O st), 851, 805 (ar C-C γ and P-C st), 758, 700 (C-F δ, CF_3, C-H δ oop and ar C-C γ). ESI-MS (positive mode +), m/z: 1433.29 $[M+ACN+Na]^+$, 1155.29 $[(M-TPPO)+ACN+Na]^+$, 557.15 $[2TPPO+H]^+$, 279.20 $[TPPO+H]^+$. Isotope used for calculation is ^{167}Er.

[Yb(L$_1$)$_3$(tppo)$_2$]: Elemental analysis (%) calculated for $C_{66}H_{48}F_9P_2O_8Yb$ (1375.09): C 57.65, H 3.52; Found: C 57.52, H 3.78. FT-IR (KBr) ν_{max} (cm^{-1}): 3252, 3151 (C-O, enol beyond the range), 3062 (ar C-H st), 2960, 2774, 2715, 2595 (C-H, Fermi resonance), 2474, 2419, 2326, 2249, 2123 (aromatic overtone), 2034, 1968, 1902, 1816 (comb, aromatic), 1774 (C=O st, keto form), 1614, 1579, 1525, 1478, 1443 (ar C-C st), 1384, 1310 (C-F st, CF_3), 1288 (P=O st), 1245, 1183, 1136 (C-F st, CF_3, ar C-H δ ip and R_3P=O st), 1081, 1023 (ar C-H δ ip and R_3P=O st), 992 (R_3P=O st), 937 (C-H δ oop and R_3P=O st), 848, 801 (ar C-C γ and P-C st), 750, 700 (C-F δ, CF_3, C-H δ oop and ar C-C γ). ESI-MS (positive mode +), m/z: 1439.09

$[M+ACN+Na]^+$ not detected, 1161.87 $[(M\text{-}TPPO)+ACN+Na]^+$, 557.31 $[2TPPO+H]^+$, 279.27 $[TPPO+H]^+$. Isotope used for calculation is ^{175}Yb.

$[Nd(L_2)_3(tppo)_2]$: Elemental analysis (%) calculated for $C_{66}H_{45}Cl_3F_9P_2O_8Nd$ (1449.60): C 54.69, H 3.13; Found: C 55.23, H 3.26. FT-IR (KBr) ν_{max} (cm^{-1}): 3241, 3155 (C-O, enol beyond the range), 3065 (ar C-H st), 2879, 2832, 2762, 2676, 2587 (C-H, Fermi resonance), 2501, 2381, 2334, 2287, 2221, 2128 (aromatic overtone), 2046, 2003, 1914, 1793 (comb, aromatic), 1727, 1680 (C=O st, keto form), 1602, 1572 1529, 1478 (ar C-C st), 1396, 1291 (C-F st, CF_3 and P=O st), 1248, 1186, 1143 (C-F st, CF_3 , ar C-H δ ip and R_3P=O st), 1097, 1011 (ar C-H δ ip and R_3P=O st), 945 (C-H δ oop R_3P=O st), 844 (ar C-C γ, C-Cl st and P-C st), 797, 743 (C-F δ, CF_3, C-H δ oop, ar C-C γ and C-Cl st), 661 (C-Cl st). ESI-MS (positive mode +), m/z: 1472.95 $[M+Na]^+$, 1194.68 $[(M\text{-}TPPO)+Na]$, 557.24 $[2TPPO+H]^+$, 279.09 $[TPPO+H]^+$. Isotope used for calculation is ^{145}Nd.

$[Sm(L_2)_3(tppo)_2]$: Elemental analysis (%) calculated for $C_{66}H_{45}Cl_3F_9P_2O_8Sm$ (1455.72): C 54.46, H 3.13; Found: C 54.86, H 3.38. FT-IR (KBr) ν_{max} (cm^{-1}): 3248, 3155 (C-O, enol beyond the range), 3069 (ar C-H st), 2922, 2882, 2835, 2769, 2676, 2591 (C-H, Fermi resonance), 2501, 2376, 2326, 2283, 2221, 2124 (aromatic overtone), 2042, 2011, 1914, 1793 (comb, aromatic), 1723, 1684 (C=O st, keto form), 1598, 1572 1532, 1481 (ar C-C st), 1400, 1295 (C-F st, CF_3 and P=O st), 1248, 1186, 1143 (C-F st, CF_3 , ar C-H δ ip and R_3P=O st), 1097, 1011 (ar C-H δ ip and R_3P=O st), 945 (C-H δ oop R_3P=O st), 844 (ar C-C γ, C-Cl st and P-C st), 797, 743 (C-F δ, CF_3, C-H δ oop, ar C-C γ and C-Cl st), 661 (C-Cl st). ESI-MS (positive mode +), m/z: 1481.15 $[M+Na]^+$, 1203.17 $[(M\text{-}TPPO)+Na]$, 557.20 $[2TPPO+H]^+$, 279.08 $[TPPO+H]^+$. Isotope used for calculation is ^{155}Sm.

$[Er(L_2)_3(tppo)_2]$: Elemental analysis (%) calculated for $C_{66}H_{45}Cl_3F_9P_2O_8Er$ (1472.62): C 53.83, H 3.08; Found: C 54.43, H 3.25. FT-IR (KBr) ν_{max} (cm^{-1}): 3229, 3155 (C-O, enol beyond the range), 3073 (ar C-H st), 2925, 2875, 2832, 2766, 2591 (C-H, Fermi resonance), 2502, 2381, 2326, 2283, 2213, 2132 (aromatic overtone), 2042, 2015, 1910, 1789 (comb, aromatic), 1727, 1680 (C=O st, keto form), 1602, 1572 1532, 1478 (ar C-C st), 1400, 1291 (C-F st, CF_3 and P=O st), 1248, 1186, 1143 (C-F st, CF_3 , ar C-H δ ip and R_3P=O st), 1097, 1011 (ar C-H δ ip and R_3P=O st), 945 (C-H δ oop R_3P=O st), 844 (ar C-C γ, C-Cl st and P-C st), 797, 747 (C-F δ, CF_3, C-H δ oop, ar C-C γ and C-Cl st), 657 (C-Cl st). ESI-MS (positive mode +), m/z: 1495.31 $[M+Na]^+$, 1217.14 $[(M\text{-}TPPO)+Na]^+$, 557.23 $[2TPPO+H]^+$, 279.08 $[TPPO+H]^+$. Isotope used for calculation is ^{167}Er.

$[Yb(L_2)_3(tppo)_2]$: Elemental analysis (%) calculated for $C_{66}H_{45}Cl_3F_9P_2O_8Yb$ (1478.42): C 53.62, H 3.07; Found: C 54.09, H 2.79. FT-IR (KBr) ν_{max} (cm^{-1}): 3248, 3155 (C-O, enol beyond the range), 3073 (ar C-H st), 2917, 2883, 2836, 2762, 2595 (C-H, Fermi resonance), 2501, 2385, 2326, 2283, 2132 (aromatic overtone), 2042, 2011, 1914, 1789 (comb, aromatic), 1727, 1680 (C=O st, keto form), 1603, 1567 1532, 1478 (ar C-C st), 1396, 1295 (C-F st, CF_3 and P=O st), 1252, 1186, 1143 (C-F st, CF_3 , ar C-H δ ip and R_3P=O st), 1093, 1011 (ar C-H δ ip and R_3P=O st), 941 (C-H δ oop R_3P=O st), 844 (ar C-C γ, C-Cl st and P-C st), 793, 739 (C-F δ, CF_3, C-H δ oop, ar C-C γ and C-Cl st), 665 (C-Cl st). ESI-MS (positive mode +), m/z: 1501.42 $[M+Na]^+$ not detected, 1223.85 $[(M\text{-}TPPO)+Na]^+$, 557.18 $[2TPPO+H]^+$, 279.09 $[TPPO+H]^+$. Isotope used for calculation is ^{175}Yb.

X-ray crystallography. For the reported structures X-ray intensity data were collected at 100 K on a Rigaku Oxford Diffraction Supernova Dual Source diffractometer equipped with an Atlas CCD detector using ω scans and Cu Kα (λ = 1.54184 Å) radiation for samples **NdL_1H_2O**, **NdL_1tppo**, **SmL_1tppo**, **SmL_2tppo** and **YbL_2H_2O**. The images were interpreted and integrated with the program CrysAlisPro (Rikagu Agilent Technology).[29] Using Olex2 [30], the structure was solved by direct methods using the ShelXS structure solution program and refined by full-matric least-squares on F^2 using the ShlelXL program package.[31] Non-hydrogen atoms were anisotropically refined and the hydrogen atoms in the riding mode and isotropic temperature factors fixed at 1.2 times U(eq) of the parent atoms (1.5 times for methyl and hydroxyl groups).

CCDC 1948500-1948504 contain the supplementary crystallographic data for this paper. These data can be obtained free of charge via www.ccdc.cam.ac.uk/data_request/cif, by emailing data_request@ccdc.cam.ac.uk, or by contacting The Cambridge Crystallographic Data Centre, 12 Union Road, Cambridge CB2 1EZ, UK; fax: +44 1223 336033.

Characterization. Photoluminescence measurements were performed on an Edinburgh Instruments FLSP920 UV-vis-NIR spectrofluorimeter setup. A 450W xenon lamp was used as the steady-state excitation source. Time-resolved measurements were recorded using a 60W pulsed xenon lamp operating at a frequency of 100 Hz, or using a Nd:YAG Continuum Surelite I laser (450 mJ @ 1064 nm), operating at a pulse rate of 10 Hz and using the third harmonic (355 nm) as the excitation source. A Hamamatsu R5509-72 photomultiplier tube was used to detect emission in the NIR region. All luminescence measurements were recorded at room temperature. Crystals were put between quartz plates (Starna cuvettes for powder samples, type 20/C/Q/0.2). Fourier Transform Infrared (FTIR) spectra were acquired in the region of 400-4000 cm^{-1} with a Thermo Scientific Nicolet 6700 FT-IR spectrometer equipped with a nitrogen-cooled Mercury Cadmium Telluride (MCT) detector and KBr beam splitter: samples were measured in KBr pellets. UV-Vis-NIR absorption spectra were acquired in the 350-2000 nm range with a Perkin Elmer Lambda 950 spectrometer, in quartz cuvette with 10 mm path length (Starna cuvette type 23/Q/10). Solution concentrations for the complexes with general formula **$LnL_{1(2)}H_2O$** was $5 \cdot 10^{-3}$ mol L^{-1} and for complexes with without water **$LnL_{1(2)}tppo$** was $1 \cdot 10^{-2}$ mol L^{-1} in chloroform-d and for complexes containing water DMSO-d^6 was added in small amount for solubility. Diffuse absorbance (DA) spectra were acquired in the 200-2000 nm range with a Varian Cary 5 spectrometer equipped with a 150 mm diameter integrating sphere on samples dispersed on Teflon film. Spectra were quantitatively rescaled to the absorption cross/section by normalizing to solution spectra taking as reference a Ln peak not overlapping with the background, under the assumption that the oscillator strength remains constant in solution and in the solid state. Elemental analysis (C, H, N) was performed on a Thermo Flash 2000 elemental analyzer, V_2O_5 was used as catalyst. ESI-MS was performed on acetonitrile (ACN) solutions with an Agilent 6230 time-of-flight mass spectrometer (TOF-MS) equipped with a Jeatstream ESI source and positive ionization mode was used.

Acknowledgements

FA acknowledges the FWO (Research Foundation Flanders) and the European Union's Horizon 2020 programme for a [Pegasus]^2 Marie Skłodowska-Curie fellowship "Nanocomposite materials for highly efficient sensitized lanthanide emission". DM thanks the Ghent University Special Research Fund (BOF) for a PhD grant (BOF15/24J/049). KVH thanks the Hercules Foundation (project AUGE/11/029 "3D-SPACE: 3D Structural Platform Aiming for Chemical Excellence") and the Special Research Fund (BOF) – UGent (project 01N03217) for funding. Thanks are due to Funda Aliç for performing CHN measurements.

Keywords: Lanthanides • Long lived emission • Quenching • NIR emission

[1] a) J.-C. G. Bünzli in *Handbook on Physics and Chemistry of Rare Earths, Vol. 50* (Eds: J.-C. G. Bünzli, K. V Pecharsky), Elsevier B.V., Amsterdam, **2016**, pp. 141-176. b) J.-C. G. Bünzli, S. V. Eliseeva, *J. Rare Earths* **2010**, *Vol. 28 (6)*, 824-842; c) S. V. Eliseeva, J.-C. G. Bünzli, *New J. Chem.* **2011**, *35*, 1165-1176; d) M. A. Katkova, M. N. Bochkarev, *Dalton Trans.* **2010**, *39*, 6599-6612.

[2] a) B. M. van der Ende, L. Aarts, A. Meijerink, *Phys. Chem. Chem. Phys.* **2009**, *11*, 11081-11095; b) J. Feng, H. Zhang, *Chem. Soc. Rev.* **2013**, *42*, 387-410, c) L. Armelo, S. Quici, F. Barigelletti, G. Accorsi, G. Bottaro, M. Cavazzini, E. Tondello, *Coord. Chem. Rev*. **2010**, *254*, 487-505; d) A. D'Aléo, F. Pointillant, L. Ouahab, C. Andraud, O. Maury, . *Coord. Chem. Rev.* **2012**, *256*, 1604-1620.

[3] a) Y. Yang, P. Wang, L. Lu, Y. Fan, C. Sun, L. Fan, C. Xu, A. M. El-Toni, M. Alhoshan, F. Zhang, *Anal. Chem.* **2018**, *90*, 7946-7952; b) Y. Li, X. Li, Z. Xue, M. Jiang, S. Zeng, J. Hao, *Biomaterials* **2018**, *169*, 35-44; c) Z. Yi, X. Li, Z. Xue, X. Liang, W. Lu, H. Pen, H. Liu, S. Zeng, J. Hao, *Adv. Funct. Mater.* **2015**, *25*, 7119-7129; d) F. Wu, H. Su, X. Zhu, K. Wang, Z. Zhang, W.-K. Wong, *J. Mater. Chem. B* **2016**, *4*, 6366-6372.

[4] a) A. Foucault-Collet, C. M. Shade, I. Nazarenko, S. Petoud, S. V. Eliseeva, *Angew. Chem. Int. Ed.* **2014**, *53*, 2927-2930; b) A. J. Amoroso, S. J. A. Pope, *Chem. Soc. Rev.* **2015**, *44*, 4723-4742; c) K. Nchimi-Nono, D. K. Wenger, S. Linden, A. Lecointre, L. Ehret-Sabatier, S. Shakir, N. Hildebrandt, L. J. Charbonnier, *Org. Boimol. Chem*. **2013**, *11*, 6493-6501.

[5] T. Förster, *Discuss. Faraday Soc.* **1959**, *27*, 7-17.

[6] a) I. Hernández , W. P. Gillin, *in Handbook on Physics and Chemistry of Rare Earths, Vol. 47* (Eds: J.-C. G. Bünzli, K. V Pecharsky), Elsevier B.V., Amsterdam, **2015**, pp.1-100; b) S. Comby, J.-C. G. Bünzli, *in Handbook on Physics and Chemistry of Rare Earths, Vol. 37* (Eds: K. A. Gscheidner, Jr., J.-C. G. Bünzli, K. V Pecharsky), Elsevier B.V., Amsterdam, **2007**, pp.217-470.

[7] E. Kreidt, C. Kruck, M. Seitz, *Handbook on Physics and Chemistry of Rare Earths, Vol. 53* (Eds: J.-C. G. Bünzli, K. V Pecharsky), Elsevier B.V., Amsterdam, **2018**, pp. 35-79.

[8] F. Quochi, R. Orrù, F. Cordella, A. Mura, G. Bongiovanni, F. Artizzu, P. Deplano, L. M. Mercuri, L. Pilia, A. Serpe, . *J. App. Phys.* **2006**, *99*, 053520.

[9] a) J.-Y. Hu, Y. Ning, Y.-S. Meng, J. Zhang, Z.-Y. Wu, S. Gao, J. L. Zhang, *Chem. Sci.* **2017**, *8*, 2702-2709; b) G. A. Kumar, R. E. Riman, L. A. Diaz Torres, O. Barbosa Garcia, S. Banerjee, A. Kornienko, J. G. Brennan, *Chem. Mater.* **2005**, *17*, 5130-5135.

[10] A. Monguzzi, A. Milani, L. Brambillia, R. Tubino, C. Castellano, F. Demartin, F. Meinardi, C. Castiglioni, *Synth. Met.* **2012**, *161*, 2693-2699.

[11] K. Scholten, A. G. Rosser, J. Wahsner, N. Alzakhem, C. Bischof, F. Stog , A. Beeby, M. Seitz, . *J. Am. Chem. Soc.* **2012**, *134*, 13915-13917.

[12] C. Bischof, J. Wahsner, J. Scholten, S. Trosien, M. Seitz, *J. Am. Chem. Soc.* **2010**, *132*, 14334-14335.

[13] R. H. C. Tan, M. Motevalli, I. Abrahams, P. B. Wyatt, W. P. Gillin, *J. Phys. Chem. B* **2006**, *110*, 24476-24479.

[14] a) C. Doffek, N. Alzakhem, C. Bischof, J. Wahsner, T. Güden-Silber , J. Lügger, C. Platas-Inglesias, M. Seitz, *J. Am. Chem. Soc.* **2012**, *134*, 16413-16423; b) P. B. Glover, A. P. Bassett, P. Noeckemann, B. M. Kariuki, R. Van Deun, Z. Pikramenou, *Chem. Eur. J.* **2007**, *13*, 6308-6320; c) J.-C. G. Bünzli, A.-S. Chauvin, H. K. Kim, E. Deiters, S. V. Eliseeva, *Coord. Chem. Rev.* **2010**, *254*, 2623-2633; d) F. Artizzu, M. L. Mercuri, A. Serpe, P. Deplano, *Coord. Chem. Rev.* **2011**, *255*, 2514-2529.

[15] J.-C. G. Bünzli, *Coord. Chem. Rev*. **2015**, *293*, 19-47.

[16] a) K. Binnemans, *Handbook on Physics and Chemistry of Rare Earths, Vol. 35* (Eds: A. K. Jr. Gschneider, J.-C. G. Bünzli, K. V Pecharsky), Elsevier B.V., Amsterdam, **2005**, pp.107-272; b) J. D. Bray, K. J. Clegg, F. L. Lindoy, D. Shilter, *Advances in Inorganic Chemistry*. **2006**, *59*, 1-37; c) D. Mara, F. Artizzu, B. Laforce, L. Vincze, K. Van Hecke, R. Van Deun, A. M. Kaczmarek, *J. Lumin*. **2019**, *213*, 343-355; d) X. Guo, H. Guo, L. Fu., L. D. Carlos, R. A.S. Ferreira, L. Sun, R. Deng, H. Zhang, *J. Phys. Chem. C* **2009**, *113*, 12538-1254.

[17] a) T. M. George, S. Varughese, M. L. P. Reddy, *RSC Adv.* **2016**, *6*, 69509-65920; b) J.-S. Kang, K. T. Leung, M.-K. Nah, J.-S. Shin, M.-H. Kang, B. Shong, J.-G. Kang, J. Lee, Y. Sohn, *New J. Chem.* **2016**, *40*, 9702-9710; c) A. N. Swinburne, M. H. Langford Paden, T. L. Chan, S. Randall, F. Ortu, A. M. Kenwright, L. S. Natrajan, *Inorganics* **2016**, *4*, 27.

[18] J.P. Martins,P. Martín-Ramos, P. Chamorro-Posada, P. S. Pereira Silva, J. Martín-Gil, S. Hernández-Navarro, M. Ramos Silva, *Adv. Cond. Matter. Phys.* **2015**, *vol. 2015*, Article ID 205047.

[19] a) F. Quochi, F. Artizzu, M. Saba, F. Cordella, M. L. Mercuri, P. Deplano, M. A. Loi, A. Mura, G. Bongovanni, *J. Phys. Chem. Lett.* **2010**, *1*, 141-144; b) H.-Q. Ye., Y. Peng, Z. Li, C.-C. Wang, Y.-X. Zheng, M. Montevalli, P. B. Wyatt, W. P. Gillin, I. Hernández, *J. Phys. Chem C* **2013**, *117*, 23970-23975; c) G. Mancino, A. J. Ferguson, A. Beeby, N. J. Long, T. S. Jones, *J. Am. Chem. Soc.* **2005**, *127*, 524-525; d) H. Q. Ye, Z. Li, Y. Peng Y, C.-C. Wang, T. Y. Li, Y. X. Zheng, A. Sapelkin, G. Adamopoulos, I. Hernández, P. B. Wyatt, W. P. Gillin, *Nat. Mater.* **2014**, *13*, 382-286.

[20] a) Y. Peng, H. Ye, Z. Li, M. Montevalli, I. Hernández, W. P. Gillin, P. B. Wyatt, *J. Phys. Chem. Lett.* **2014**, *5*, 1560-1563; b) A. Mech, A. Monguzzi, F. Meinardi, J. Mezyk, G. Macchi, R. Tubino, *J. Am. Chem. Soc.* **2010**, *132*, 4574-5476; c) L. Winkless, R. H. C. Tan, Y. Zheng, M. Montevalli, P. B. Wyatt, W. P. Gillin, *App. Phys. Lett.* **2006**, *89*, 111115; d) A. Monguzzi, R. Tubino, F. Meinardi, A. O. Biroli, M. Pizzotti, F. Demartin, F. Quochi, F. Cordella, A. M. Loi, *Chem. Mater.* **2009**, *21*, 128-135.

[21] a) R. Pizzoferrato, R. Francini, S. Pietrantoni, R. Paolesse, F. Mandoj, A. Monguzzi, F. Meinardi, *J. Phys. Chem. A* **2010**, *114*, 4163-4168; b) C. Yu, Z. Zhang, L. Liu, H. Li, Y. He, X. Lü, W.-K. Wong, R. A. Jones, *New J. Chem.* **2015**, *39*, 3698-3707; c) Z. Ahmed, K. Iftikhar, *J. Phys. Chem. A* **2013**, *117*, 11183-11201; d) B. L. Reid, S. Stagni, J. M. Malicka, M. Cocchi, A. N. Sodolev, B. W. Skelton, E. G. Moore, G. S. Hanan, M. I. Ogden, M. Massi, *Chem. Eur. J.* **2015**, *21*, 18354-18363.

[22] a) E. R. Trivedi, S. V. Eliseeva, J. Jankolovits, M. M. Olmstead, S. Petoud, L. Pecoraro, *J. Am. Chem. Soc.* **2014**, *136*, 1526-1534; b) C. Doffek, N. Alzakhem, M. Molon, M. Seitz, *Inorg. Chem.* **2012**, *51*, 4539-4545; c) X. Yang, D. Schipper, R. A. Jones, L. A. Lytwak, B. J. Holliday, S. Huang, *J. Am. Chem. Soc.* **2013**, *135*, 8468-8471.

[23] a) N.M. Shavaleev, R. Scopelliti, F. Gumy, J.-C. G. Bünzli, *Eur. J. Inorg. Chem.* **2008**, *9*, 1523-1529; b) W. Li, P. Yan, G. Hou, H. Li, G. Li, *RSC Adv.* **2013**, *3*, 18173-18180; c) Z. Zhang, W. Feng, P. Su, X. Lü, J. Song, D. Fan, W.-K. Wong, R. A. Jones, G. Su, *Inorg. Chem.* **2014**, *53*, 5950-5960; d) B. Branchi, P. Ceroni, V. Balzani, F.-G. Klärner, F. Vögth, *Chem. Eur. J.*, **2010**, *16*, 6048-6055.

[24] a) L. A. Galán, A. N. Sobolev, B. W. Skelton, E. Zysman-Colman, M. I. Ogden, M. Massi, *Dalton Trans.* **2018**, *47*, 12345-12352; b) Z. Zhang, S. Petoud, *Chem. Eur. J.* **2008**, *14*, 1264-1272; c) Z. Ahmed, K. Iftikhar, *Dalton Trans.* **2019**, *48*, 4973-4986; d) N. M. Shavaleev, R. Scopelliti, F. Gumy, J.-C. G. Bünzli, *Inorg. Chem.* **2008**, *47*, 9055-9068.

[25] Z. Ahmed, K. Iftikhar, *Polyhedron.* **2015**, *85*, 570-592.

[26] A.P.Pushkarev, A. N. Yablonskiy, P. A. Yunin, M. E. Burin, B. A. Andreev, M. N. Bochkarev, *Spectroc. Acta Pt. A-Molec. Biomolec. Spectr.* **2016**, *163*, 134-139.

[27] a) A. Sanguineti, A. Monguzzi, G. Vaccuro, F. Meinardi, E. Ronchi, M. Moret, U. Cosentino, G. Moro, R. Simonutti, M. Mauri, R. Tubino, L. Beverina, *Phys. Chem. Chem. Phys.* **2012**, *14*, 6452-6455; b) C. Kruck, P. Nazari, C. Dee, S. B. Richards, A. Turshatov, M. Seitz, *Inorg. Chem.* **2019**, *58*, 6959-6965; c) X.-S. Ke, B.-Y. Yang, X. Cheng, S. L.-F. Chan, J.-L. Zhang, *Chem. Eur. J.* **2014**, *20*, 4324-4333; d) S. Biju, Y. K. Eom, J.-C. G. Bünzli, H. K. Kim, . *J. Mater. Chem. C* **2013**, *1*, 6935-6944.

[28] a) B. Li, P. Chen, W. Sun, C. Wang, T. Gao, P. Yan, *Phys. Chem. Chem. Phys.* **2015**, *17*, 30510-30517; b) C. Doffek, M. Seitz, *Angew. Chem. Int. Ed.* **2015**, *54*, 9719-9721; c) S. A. Bhat, K. Iftikhar, *J. Lumin.* **2019**, *208*, 334-341; d) I. Hernández, Y.-X. Zheng, M. Montevalli, R. H. C. Tan, W.

10.1002/chem.201904320

P. Gillin, P. B. Wyatt, *Chem. Commun.* **2013**, *49*, 1933-1935; e) H. He, P. S. May, D. Galipeau, *Dalton Tans.* **2009**, *24*, 4766-4771.

[29] Rigaku Oxford Diffraction. **2015**, CrysAlis Pro; Rigaku Oxford Diffraction, Yarnton, England.

[30] O. V. Dolomanov, L. J. Bourhis, R. J. Gildea, J. A. K. Howard, H. Puschmann, *J. Appl. Crystallography* **2009**, *42*, 339-341.

[31] a) G. M. Sheldrick, *Acta Crystallogr., Sect. A: Found. Crystallogr.* **2008**, *64*, 112-122; b)) G. M. Sheldrick, *Acta Crystallogr. Sect. C* **2015**, *71*, 3-8.

10.1002/chem.201904320

WILEY-VCH

Entry for the Table of Contents

Layout 1:

FULL PAPER

Replacement of coordinated water molecules with tppo ligands in Ln complexes overcomes CH quenching and boosts NIR emission.

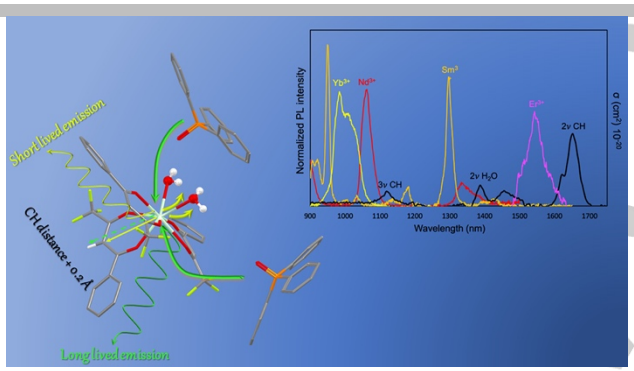

*Dimitrije Mara,[a,b] Flavia Artizzu, *[a] Philippe F. Smet,[c] Anna M. Kaczmarek,[d] Kristof Van Hecke,[b] and Rik Van Deun[a]*

Page No. – Page No.

Vibrational Quenching in Near-Infrared Emitting Lanthanide Complexes: A Quantitative Experimental Study and Novel Insights